THE JOURNAL OF PHYSICAL CHEMISTRY A
A JOURNAL OF THE AMERICAN CHEMICAL SOCIETY

pubs.acs.org/JPCA Article

Various Sorts of Chalcogen Bonds Formed by an Aromatic System

Steve Scheiner*

Cite This: J. Phys. Chem. A 2022, 126, 4025−4035 Read Online

ACCESS | Metrics & More | Article Recommendations | Supporting Information

ABSTRACT: The chalcogen Y atom in the aromatic ring of thiophene and its derivatives YC_4H_4 (Y = S, Se, Te) can engage in a number of different interactions with another such unit within the homodimer. Quantum calculations show that the two rings can be oriented perpendicular to one another in a T-shaped dimer in which the Y atom accepts electron density from the π-system of the other unit in a Y···π chalcogen bond (ChB). This geometry best takes advantage of attractions between the electrostatic potentials surrounding the two monomers. There are two other geometries in which the two Y atoms engage in a ChB with one another. However, instead of a simple interaction between a σ-hole on one Y and the lone pair of its neighbor, the interaction is better described as a pair of symmetrically equivalent Y···Y interactions, in which charge is transferred in both directions simultaneously, thereby effectively doubling the strength of the bond. These geometries differ from what might be expected based simply on the juxtaposition of the electrostatic potentials of the two monomers.

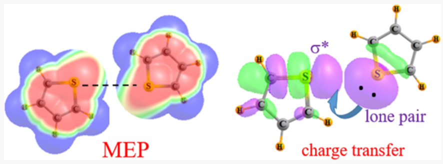

■ INTRODUCTION

The interactions between molecules play an enormous role in chemistry and biology. These interactions take many forms, from very simple and weak van der Waals type[1−3] to much stronger ones involving charged species.[4−10] The H-bond represents a middle ground, with energies generally in the range between about 3 and 15 kcal/mol.[1,11−14] However, its modest strength belies its enormous importance, from maintaining the genetic code of all life on the planet to mediating the chemical reactions that take place within cells and the oceans. Its importance has motivated more than a century of study of the origin and influence of the H-bond, which is still capable of offering new insights into its character and influence.

There has been a recent flurry of activity in the identification and study of a set of noncovalent bonds that bear strong resemblance to the H-bond.[15−22] These bonds depart from the H-bond pattern in that the bridging H is replaced by any of a set of nominally more electronegative atoms. However, despite this difference, these bonds are characterized by very similar underlying forces, viz. electrostatic attraction, coupled with polarization, charge transfer, and dispersion. This entire set of attractive interactions is typically placed into categories where the bond carries the name of the column of the periodic table from which the bridging atom is derived, as for example halogen, pnictogen, or tetrel bonds.

The chalcogen bond (ChB) that involves S, Se, and Te is a particularly interesting member of this family. Although not commonly considered in the older literature, there were instances of this interaction occurring, even if not formally recognized under this rubric at the time.[23] Its presence and influence is currently being demonstrated in a startling number of different sorts of systems.[24−32] In its typical divalent bonding pattern, a chalcogen (Y) atom is connected to two R substituents and also carries two lone electron pairs in an overall tetrahedral arrangement, as in the simple example of SMe_2. Each substituent would generate a σ-hole along the extension of the R-Y axis, which could engage in a ChB with an approaching nucleophile, but the position and strength of each such σ-hole would be mediated by its neighboring Y lone pairs. The ChB in which such divalent YR_2 molecules participate has been the subject of some substantial probing, and much has been learned as a result. Its presence was perhaps first detailed by surveys of crystal structures in the CSD[33] and in thiazole and selenazole nucleosides,[34] as well as in an intramolecular setting.[35] Other characteristics were obtained from the work by the Iwaoka group[36] that focused on cystine and methionine groups within proteins.[37] Sanz et al.[38,39] focused on the topology of the charge density, while others stressed the importance of the electrostatic potential surrounding the molecule[40] or the alignment of the lone pair on one unit with an antibonding orbital on the other.[41−43] In an interesting aside, other investigations have demonstrated how such bonds could figure into curious square motifs, which lead to unique supramolecular structures.[44−48]

Less studied to this point has been the sort of ChBs in which hypervalent chalcogen atoms participate.[49−51] As one example, SF_4 appears to engage in ChBs of strength roughly comparable to that of its divalent SF_2 analogue although the former undergoes a larger molecular deformation upon complexation[52] and either can engage in a ChB with a π-electron system as

Received: April 10, 2022
Revised: June 7, 2022
Published: June 22, 2022

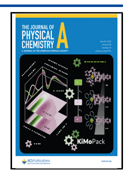

https://doi.org/10.1021/acs.jpca.2c02451
J. Phys. Chem. A 2022, 126, 4025−4035

electron donor[53] although SF_2 is preferred. Whether divalent or tetravalent, the bond strength rises quickly[54] as the Y atom grows in size: S < Se < Te. However, the hexavalent bonding scenario around a YF_6 molecule weakens any such bond to the point that its presence is questionable.[54]

A particularly interesting and unique bonding pattern for a chalcogen atom places it within an aromatic unit. The YC_4H_4 ring of thiophene and its derivatives presents a 6-e aromatic π-system,[55] wherein each C contributes a single π electron, and two more are added by the p_π orbital of Y. Unlike most other chalcogen-containing molecules, the Y atom here contains a single lone pair, oriented along the bisector of the C−Y−C angle and within the molecular plane. Each of the two C−Y bonds ought to generate a σ-hole, also within the plane of the molecule. Hence, in principle, a pair of such YC_4H_4 molecules should be able to engage in a Y···Y chalcogen bond, pairing the lone pair of one unit with a σ-hole of the other. However, the calculations presented here belie this expectation, finding a number of dimer geometries, all of which contain elements of a ChB, but none correspond to the anticipated one-to-one interaction between a σ-hole of one Y atom and a lone pair of the other. Some of the complexes are stabilized by a Y···π ChB and others by a Y···Y ChB primarily involving the σ-systems. The calculations propose the new concept of a Y···Y ChB, which is in some sense a double ChB: charge is transferred from the lone pair of one Y to the σ* antibonding orbital of the other, and an equal amount is simultaneously transferred in the reverse direction.

■ METHODS

Quantum chemical calculations were carried out with the aid of the Gaussian 16[56] suite of programs. Density functional theory, with the M06-2X functional,[57] was used in conjunction with the aug-cc-pVDZ basis set, which includes both polarization and diffuse functions along with a double-ζ foundation. The accuracy of this approach has been confirmed by numerous past calculations of related systems.[48,58−61] The aug-cc-pVDZ-PP pseudopotential[62] represented the fourth-row Te as it takes into account certain relativistic effects.

Geometries were fully optimized, with all positive vibrational frequencies confirming them as true minima. The interaction energy E_{int} is defined as the difference between the energy of the dimer and the sum of the energies of the two monomers in the geometry they adopt within the complex; this quantity was corrected for basis set superposition error by the standard counterpoise protocol.[63] The Multiwfn program[64] permitted graphic illustration of the total densities and the electron localization functions (ELFs); the maxima and minima of the molecular electrostatic potential (MEP) were assessed on an isodensity surface of ρ = 0.001 a.u. The Atoms in Molecules (AIM) method identified bond paths, and the properties of their bond critical points, in the context of the AIMAll[65] program. Individual orbitals, and the energetic contributions of charge transfers between them, were assessed by natural bond orbital (NBO) theory[66,67] via the NBO3 program incorporated into Gaussian. Total interaction energies were decomposed into physically meaningful components by the symmetry-adapted perturbation theory (SAPT) protocol[68,69] with the aid of the MOLPRO program,[70] within the context of the aug-cc-pVDZ basis set.

■ RESULTS

Properties of Monomers. It would be instructive to first examine the salient properties of the five-membered ring molecules YC_4H_4, where Y refers to S, Se, and Te. O was not included as it very seldom participates in a chalcogen bond and only in exceptional circumstances. Figure 1a depicts the total

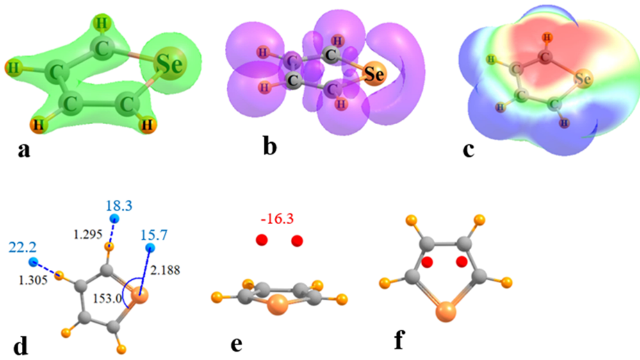

Figure 1. (a) Total electron density on 0.18 au contour. (b) ELF diagram on 0.8 contour. (c) MEP surrounding SeC_4H_4 on a surface corresponding to 1.5 × vdW radii of atoms. Blue and red colors, respectively, correspond to +12.5 and −12.5 kcal/mol. (d) Positions of V_{max} on the 0.001 au isodensity surface in the molecular plane, with values shown in blue in kcal/mol. (e and f) Two views of positions of V_{min} shown as red discs, with values in kcal/mol. Distances in Å, angles in degs.

electron density of selenophene SeC_4H_4 as an example, which contains a gap in the density between Se and its two adjacent C atoms, suggesting that the aromaticity does not fully incorporate the Se electrons into the π-system. This idea is consistent with the three C−C bond lengths, which are not equal to one another. The two C−C bond lengths adjacent to Se are 1.363 Å, as compared to a longer 1.434 Å for the third C−C bond, opposite to Se. Rather than a full integration of Se into the π-system, the electronic structure leans toward one where Se interacts with a conjugated −C═C−C═C− butadiene system. Nonetheless, the molecule is an aromatic one. The NICS(1) index, as measured by the negative of the nuclear magnetic resonance (NMR) chemical shielding of a point lying 1.0 Å above the molecular center, is −10.1 ppm (−10.5 and −9.0 ppm for Y = S and Te, respectively). This order of decreasing aromaticity (S > Se > Te) conforms to a previous study of these three molecules based on NMR, diamagnetic susceptibility, dipole moment, and structural data.[55] These NICS values compare favorably with a shielding of −10.0 ppm in the fully aromatic benzene.

The ELF diagram in Figure 1b focuses on electron pairs. The plot suggests that the classical Se lone pair in the molecular plane coalesces with its p_π orbital, which formally engages with the ring π-system to form an extended region of electron density. The manner in which the electron density produces the MEP is illustrated in Figure 1c where the red and blue regions, respectively, indicate negative and positive areas of the MEP. The MEP is most positive in the molecular plane and corresponds to the four H atoms in the plane of the molecule; there is an additional positive area along the extensions of the C−Se bonds, which correspond to σ-holes. Note, however, that these holes tend to coalesce with the positive MEP emanating from the neighboring H atoms. A detailed analysis of an isodensity surface with ρ = 0.001 au yields four CH maxima and two Se σ-holes, as illustrated in Figure 1d. V_{max} is equal to 15.7

https://doi.org/10.1021/acs.jpca.2c02451
J. Phys. Chem. A 2022, 126, 4025−4035

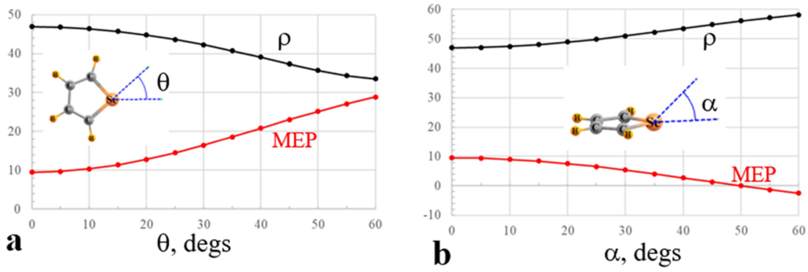

Figure 2. Variation of the electron density (10^{-4} au) and MEP (kcal/mol) 1.8 Å from the Se atom (a) in and (b) out of the molecular plane.

kcal/mol for the two σ-holes, a little larger, 18.3 kcal/mol, for the neighboring CH, and larger still at 22.2 kcal/mol for the CH groups that are not adjacent to Se. The MEP is generally negative above the molecular plane. The minima reside more or less above the two C−C bonds as shown in Figure 1e,f, with values of −16.3 kcal/mol. The absence of minima above the Se−C bonds may be connected with the gap in the π-electron density evident in Figure 1a. Figure S5 presents analogous diagrams for Y = S and Te, where the similarities with selenophene are obvious.

Figure 2 provides a more quantitative view of the MEP centered around the Se atom. So as to be consistent with the Se vdW bond radius,[71] the data in Figure 2 were collected at a distance of 1.8 Å from the Se nucleus. As may be seen in Figure 2a, the density declines as the reference point is displaced off of the C−Se−C bisector, in the approximate location of the Se lone pair, in the molecular plane. This drop of ρ causes a steady rise in the MEP, which nearly triples as a result of a 60° displacement. In contrast to this behavior, Figure 2b shows that displacement out of the molecular plane increases the density, such that the MEP suffers a lowering, to the point that the MEP reverses its sign for displacements of more than 50°. These behaviors are consistent with diagrams in Figure 1. The MEPs of thiophene and tellurophene presented in Figure S5 are quite similar to those in Figure 2.

Another perspective on the electronic structure surrounding this molecule arises from adding a small base or acid of moderate strength, so that one can further probe the molecule so as to see where each of these molecules prefers to situate itself. The NH_3 base finds two locations around SeC_4H_4, and these minima are displayed in Figure 3a,b. The first takes advantage of both the Se

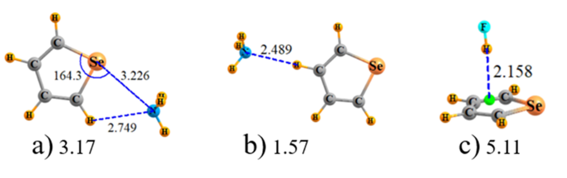

Figure 3. Minima on the potential energy surface combining SeC_4H_4 with (a, b) NH_3 as the base and (c) HF as the HB donor; the green dot represents the midpoint of the indicated C−C bond. Numbers refer to interaction energy in kcal/mol; distances in Å; and angles in degs.

σ-hole and the CH positive region, wherein NH_3 engages in both a chalcogen and H-bond. The total interaction energy is 3.17 kcal/mol. Although the positive region around the more distant CH is a bit deeper, the interaction energy for the CH···N H-bond in Figure 3b is a bit smaller, since there is no auxiliary chalcogen bond. The strongest interaction of all occurs when HF approaches above the molecular plane in Figure 3c, with an interaction energy of 5.11 kcal/mol. The HF situates itself very close to the position of V_{min} in Figure 1, above one of the C−C bonds. Although the red region in Figure 1c seems to span the entire molecule, it is only the geometry depicted in Figure 3c that represents a minimum with HF as the partner. When initially placed near the Se lone pair, so that an FH···Se H-bond is possible, the HF migrates above the ring.

Types of Dimer Structures. Inspection of the spatial disposition of the MEP around the various YC_4H_4 monomers permits some educated guesses as to the geometries that might be expected if two of these molecules are paired with one another. In particular, the positive blue areas around the rim of the molecule ought to be attracted toward the negative red region lying above the molecular plane. As such, a T-shaped homodimer would be the expected result. This idea is reinforced by the strong complex illustrated in Figure 3c where an FH molecule approaches the molecular plane from above.

T-Shaped Dimers. However, these ideas are unable to refine the structure beyond this generic ideal. For this purpose, the two molecules were placed in various configurations relative to one another, followed by full geometry optimization. For each of the Y atoms, S, Se, and Te, there were three perpendicular minima located on the potential energy surface. These optimized geometries are displayed in Figure 4a−c for the case of

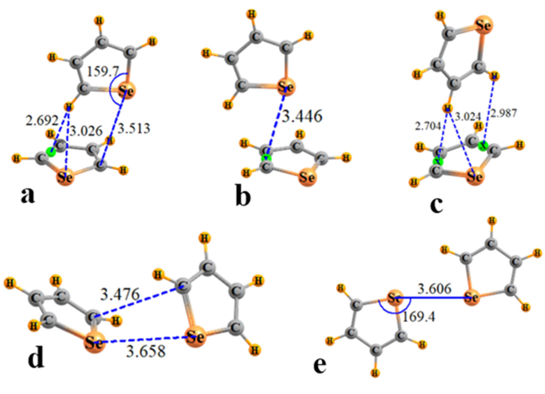

Figure 4. (a−e) Optimized homodimers of SeC_4N_4. The green dot represents the midpoint of the indicated C−C bond; distances in Å and angles in degs.

selenophene Y = Se. Based only on the geometries, it is difficult to judge which atoms of the two monomers interact with one another. Each of the broken blue lines in Figure 4 refers to a bond path derived from AIM analysis. In some cases, the terminus of a bond path leads to a bond, rather than a single atom. For each such instance, a green disk indicates the position of the midpoint of that bond. The actual AIM diagrams in Figure S1a−c indicate that the density at each bond critical point is on the order of 0.007 au. In terms of the atoms connected to one another, one could identify what look like both chalcogen and

https://doi.org/10.1021/acs.jpca.2c02451
J. Phys. Chem. A 2022, 126, 4025−4035

H-bonds in these structures. The presence of these noncovalent bonds is further verified by the NCI diagrams in Figure S1d−f.

NBO analysis of the global minimum of Figure 4a is generally consistent with the AIM diagram. For example, the chalcogen bond is supported by $E(2)$ of 0.72 kcal/mol. The H-bonds are verified by $E(2)$ contributions to the $\sigma^*(CH)$ antibonding orbital, e.g., 1.3 kcal/mol from the C−C π-bond. Hence, in summary, NBO reinforces the idea that the stronger H-bonding is supplemented by a weaker chalcogen bond. On the other hand, it might be an oversimplification to focus too closely on particular bond paths, as the bonding pattern seems to spread out over the entire breadth of the π-system of the lower molecule, as indicated by the NCI diagram in Figure S1d.

Another T-shaped dimer is displayed in Figure 4b in which the upper molecule slides to the left, relative to Figure 4a. This motion leaves only a single AIM bond path, a chalcogen bond to a π(CC) bond, with ρ_{BCP} = 0.0074 au. A third geometry in Figure 4c rotates the upper molecule so that it approaches the lower with a pair of CH bonds, leading to several H-bonds involving either a C═C bond or Se as the electron donor. Figure S1c lists their bond critical point densities as lying in the range between 0.0053 and 0.0073. Although AIM identifies different numbers of specific noncovalent bonds in each T-dimer, the NCI diagrams in Figure S1d−f are rather similar to one another, suggestive of an overall delocalized bonding that covers a full area of the lower molecule's π-cloud.

The S and Te analogues of these homodimers exhibit very similar geometries, all of which are depicted in Figure S2. There are some distinctions between the three Y atoms in terms of specific AIM bond paths, but the overall patterns are quite similar, especially the delocalized NCI bonding region.

The energetics of these perpendicular dimers are reported in the first three rows of Table 1. Dimer **a** is most stable of the three, followed by **b** and then **c**, although all have energies within about 2 kcal/mol of one another. It is perhaps notable that structure **c** has the highest energy even though V_{max} is the largest for the CH group which is involved in a H-bond in that geometry (see Figure 1d). The next three columns of Table 1 delineate the interaction energies of each dimer (corrected for basis set superposition error). The dimerization energy of structure **a** varies from 3.7 kcal/mol for Y = S up to 4.6 kcal/mol for Te, with the Se intermediate between the two. This quantity diminishes for structures **b** and **c**, consistent with their relative energies. Regardless of the particular Y atom, the most stable dimer contains a chalcogen bond as well as one or more H-bonds involving its neighboring CH group. Note that the order of interaction energy rises in the order expected for a ChB, S < Se < Te, for both structures **a** and **b**, which contain such a bond, but is insensitive to the nature of the Y atom for **c**, which contains no ChB.

Table 1. Relative Energies of Various Conformers of $(YC_4H_4)_2$ and Their Interaction Energies, All in kcal/mol

	E_{rel}			$-E_{int}$		
	S	Se	Te	S	Se	Te
a	0.0	0.0	0.0	3.69	4.01	4.60
b	1.02	0.95	0.44	2.66	3.24	4.25
c	1.09	1.39	1.86	2.74	2.66	2.72
d	1.57	1.55	1.59	2.50	2.84	3.36
e	2.46	2.80		2.26	1.49	

Slipped Stacked Structures. Another sort of stable minimum located on the surface might be described loosely as stacked but slipped, i.e., shifted relative to one another. Figure 4d illustrates this type of structure for Y = Se, with very similar shapes for S and Te, added to Figure S3. Structure **d** is symmetric in the sense that the two monomers are equivalent to one another. According to AIM, structure **d** is stabilized by a Se···Se chalcogen bond, as well as a C···C tetrel bond. Because of the symmetry, each such chalcogen bond contains equal elements of transfer from the lone pair of one molecule to the $\sigma^*(CSe)$ of its neighbor, and vice versa, so there is no net intermolecular charge transfer. The AIM picture changes slightly for thiophene where the C···C interaction is replaced by CH···S H-bonds, as pictured in Figure S3d. However, the NCI bonding regions of Figure S3 resemble one another very closely and so do not suggest any real change in the bonding pattern. NBO analysis confirms the presence of each Y···Y chalcogen bond with $E(2)$ for the $Y_{lp} \rightarrow \sigma^*(YC)$ transfer equal to 0.4, 0.7, and 1.2 kcal/mol, respectively, for Y = S, Se, and Te. It must be borne in mind, though, that an equivalent amount arises for the transfer in the opposite direction, so these quantities should effectively be doubled for a true estimate for the full chalcogen bond.

As indicated in Table 1, structure **d** is slightly higher in energy than any of the T-shaped dimers with the exception of Y = Te where **d** is slightly more stable than **c**. The interaction energies of these slipped parallel dimers are between 2.5 and 3.4 kcal/mol and follow the pattern of strengthening S < Se < Te, which is typical of chalcogen bonds. The bond length elongates in this same order, with R(Y···Y) equal to 3.560, 3.658, and 3.933 Å, respectively, as the Y atom grows larger.

Planar Structures. The fifth minimum located on these surfaces, and the least stable, places the two monomers in the same plane, as exemplified by Figure 4e. While there is such a minimum for Y = S and Se, there is no such coplanar dimer existing on the surface for Y = Te. There is a sort of dual chalcogen bond between the two Y atoms, in that the symmetry is such that each atom plays the role of the electron donor and acceptor simultaneously. For example, $E(2)$ for the $Y_{lp} \rightarrow \sigma^*(YC)$ transfer is 0.3 kcal/mol for one direction and the same amount for the other direction for Y = S; this quantity rises to 0.4 kcal/mol for Se. NBO verifies a pair of CH···S H-bonds, with $E(2)$ for $S_{lp} \rightarrow \sigma^*(SH)$ = 0.3 kcal/mol for each; as illustrated in Figure S4, AIM does not place a bond path between these atoms for Y = Se, although NBO would suggest otherwise with $E(2)$ = 0.2 kcal/mol. Indeed, the NCI diagrams in Figure S4 do not indicate much difference between the S and Se complexes, so one can attribute the stability of these planar complexes to a combination of chalcogen and H-bonds. Unlike the normal expectation for chalcogen bonds, the interaction weakens as Y grows larger and even vanishes for Te.

As a final point, the reliability of this level of theory was carefully tested for the thiophene systems. Computation of the interaction energies with a larger aug-cc-pVTZ basis set, shown in Table S1, indicates that the triple-valence set slightly reduces these quantities, but their order is unaffected. A recent study[72] has evaluated various functionals for application to chalcogen-bonded systems and found M06-2X one of the more accurate. To provide further assurance of its reliability, computations were also carried out with the ωB97-XD functional. As shown in Table S1, the interaction energies suffered only a small reduction, again keeping the energetic ordering intact.

https://doi.org/10.1021/acs.jpca.2c02451
J. Phys. Chem. A 2022, 126, 4025−4035

ANALYSIS OF BONDING

As should be evident, these dimers are held together by a variety of forces and noncovalent bonds. The perpendicular T-shaped complexes are favored by the Coulombic juxtaposition of the positive potential in the plane of the molecule with the negative region above the plane of the partner monomer. SAPT partitioning of the total interaction energy thus reveals a substantial negative electrostatic component (ES) in Table 2.

Table 2. SAPT Components (kcal/mol) of Interaction Energy of $(SC_4H_4)_2$

	a	b	c	d	e
ES	−4.12	−2.62	−2.72	−3.31	−1.48
EX	7.32	6.66	5.75	5.60	3.77
IND	−4.07	−3.39	−1.84	−3.19	−1.79
EX-IND	3.60	3.05	1.54	2.91	1.53
DISP	−6.53	−6.23	−5.71	−4.85	−3.80
EX-DISP	0.93	0.94	0.77	0.69	0.42

However, induction energy (IND) is also rather large, characteristic of the presence of noncovalent bonds. Dispersion (DISP) is even larger, which is characteristic of an overall attractive force without specific bonds as a requirement, particularly when the interaction involves the entire π-system. The decomposition of complex **b**, with the purest ChB of those in this class, has DISP as the largest component, followed by IND and ES in that order. Parenthetically, the SAPT results are insensitive to enlargement of the basis set. Expansion to aug-cc-pVTZ changes the quantities in Table 2 by only 0.03 kcal/mol, with a slightly larger increase of 0.3 kcal/mol for the dispersion contribution.

The slipped parallel dimer **d** no longer places the positive region in the plane of one unit in direct coincidence with the negative out-of-plane segment of the other, but the electrostatic component is nevertheless attractive and comparable to that in the T-shaped dimers, as is the induction. On the other hand, the switch away from the interaction with the π-cloud reduces the dispersion energy of **d**. All of these elements suffer a decline in passing over to the planar **e** dimer. The latter geometry forces the positive planar regions to face one another, so ES is only marginally attractive. Reductions in the induction and dispersion energy also occur, but the concomitant decrease in the exchange repulsion keeps the entire interaction attractive. Nonetheless, dispersion appears to make the largest contribution to the interactions within structures **d** and **e**, as was also the case with the T-dimers. It is worth noting that the high proportion of dispersion in the coplanar structure, and the weaker but attractive electrostatic term, has been confirmed in earlier calculations[73] of similar dimers extracted from X-ray structures. This similarity is of particular interest as the structures examined in this previous work had no possibility of H-bonds between the SC_4 ring units.

With regard to specific sorts of noncovalent bonds, a scan of the molecular structures, combined with AIM and NBO analysis of the wavefunctions, suggests a combination of chalcogen with hydrogen bonds, in differing proportions in the various dimers. Some of the most important parameters relative to this picture are compiled in Table 3. For perpendicular structures **a** and **b**, it is the C═C π-bond that serves as the source of electrons in the ChB, so R refers to the distance from Y to the C−C midpoint. This distance elongates as Y grows larger but is consistently shorter for structure **b** than for **a**. This sign of a stronger ChB in **b** is also consistent with the more linear θ(CY···D) (where D refers to the donor C−C midpoint). The next two columns list the bond critical point density of both the ChB and any HB bond paths that might be present. These quantities are similar for the ChB and HB in structure **a**, but it is the ChB that dominates in **b**. This same finding of a preponderant influence of the ChB in **b** may be seen as well in the NBO $E(2)$ measures of charge transfer in the last two columns of Table 3. Hence, structure **a** represents a near equal blend of ChB and HB, while dimer **b** is held together almost exclusively by a $\pi(CC) \rightarrow \sigma^*(YC)$ chalcogen bond.

The slipped parallel dimer **d** has a considerably longer ChB, but it must be stressed that this distance is that between the two Y nuclei, not to a bond midpoint. The AIM and NBO data suggest that this complex is again a mix of ChB and HB, with a slightly larger proportion of the former. Judging by the Y···Y distances and angles in Table 3, the ChB would appear to be a bit

Table 3. Comparison of Characteristics of ChB and HB[a] in Homodimers

	$-E_{int}$, kcal/mol	R(Y···D[b]), Å	θ(CY···D[b]), degs	ρ, 10^{-4} au		$E(2)$, kcal/mol	
				ChB	HB	ChB	HB
a							
S	3.69	3.424	168	68	3 × 70	0.7	1.5
Se	4.01	3.464	162	71	2 × 71	1.0	2.0
Te	4.60	3.537	156	75	72	1.3	1.7
b							
S	2.66	3.404	172	70	55	0.7	0.3
Se	3.24	3.446	166	74		1.0	0.2
Te	4.25	3.514	157	80		1.5	0.1
d							
S	2.50	3.560	154	67	2 × 57	0.4	0.3
Se	2.84	3.658	152	74	2 × 57	0.7	0.2
Te	3.36	3.933	143	73	2 × 55	1.2	0.1
e							
S	2.26	3.478	176	70	2 × 50	0.3	0.3
Se	1.49	3.606	169	71		0.4	0.2

[a]Distance and angles measured from the π(CC) midpoint in structures **a** and **b**. [b]D refers to the C−C midpoint in **a** and **b** and to other Y atom in **d** and **e**.

https://doi.org/10.1021/acs.jpca.2c02451
J. Phys. Chem. A 2022, 126, 4025−4035

stronger in planar dimer **e** than in **d**, although the AIM and NBO data do not reflect much of a difference.

One window into the strength of a CH···Y H-bond is the stretch undergone by the C−H bond upon dimerization. These stretches outlined in Table 4 certainly confirm the presence and influence of H-bonds in the perpendicular dimer **c**, where each C−H bond elongates by several mÅ. The hypothesized HBs in **a** are confirmed by stretches that are roughly 1 mÅ, while their absence in **b** is supported by the very small changes, some of them in fact small compressions. The stretches in dimer **d** are also small but consistently positive, suggestive of a weak CH···Y HB, while planar complex **e** would appear to have little to no H-bonds present. Hence, like **b**, one may consider the planar complex **e** held together primarily by a ChB with only marginal supplementation by HBs.

Table 4. Change in r(CH) (mÅ) Resulting from Formation of Dimers

	S	Se	Te
a	0.8	0.7	1.2
b	−0.5	−0.5	0.3
c	2.8	3.2	4.5
d	0.3	0.3	0.8
e	−0.3	−0.3	

Y···Y Chalcogen Bonds. Planar dimer **e** is uniquely interesting from a number of perspectives. In the first place, it would appear to place the σ^*(CY) antibonding orbital and σ-hole of one monomer in near perfect alignment with that of its partner, an unusual situation. More importantly, this structure would also displace the Y lone pair, which lies along the C−Y−C bisector of the ring away from the σ^* orbital of its partner, and minimize the overlap necessary for the charge transfer involved in a ChB. Figure 5a illustrates the relevant orbitals in the thiophene dimer and shows that the S lone pair is broad enough that its displacement does not fully disrupt the necessary overlap between these two orbitals, leaving $E(2)$ equal to 0.31 kcal/mol. Note also that as per the symmetry of this complex, there is an equivalent arrangement where the lone pair and σ^* orbitals of the two molecules are switched (see Figure 5b), so that the Y···Y ChB is reinforced by a doubling of this sort of overlap. The rotation of the Y lone pair away from the σ^*(CY) antibonding orbital has a hidden benefit as well. Although this displacement lowers its overlap with σ^*(CY), it facilitates its overlap with a σ^*(CC) orbital, as displayed in Figure 5c. With a value of $E(2)$ = 0.11 kcal/mol for this transfer, this interaction might be characterized as a weak tetrel bond. As is the case for the ChB, this tetrel bond is effectively doubled due to the symmetry of the geometry.

Another facet of the geometry of dimer **e** is that its symmetry is such that if one considers the intermolecular Y···Y axis, the MEP of one molecule along this axis must be equal in both sign and magnitude to that of the other. Figure 2a shows that the MEP is positive along this C-Y axis, for $\theta \sim 55°$, so at first blush, the electrostatic energy ought to reflect the repulsion between the two positive MEPs along this axis. However, this idea reflects a gross oversimplification of the nature of the electrostatic interaction. In the first place, there is a certain degree of charge penetration as the two molecules approach one another, which would ameliorate any repulsion. Second, the interaction is not simply a point-to-point contact along the dashed line representing the Y···Y axis of Figure 5d but must also reflect other areas of contact. While it is true that blue positive areas of Figure 5d make contact with one another along the dashed line, representing the Y···Y axis, there are other adjacent regions of contact between opposite charge or between those of much less positive charge. Hence, the rotation of the two molecules that displaces the σ^*(CY) orbital of one unit from the Y lone pair of the other, leading to the symmetry of structure **e**, allows an overall attractive electrostatic component, albeit not a very large one.

Structure **d** slides each molecule out of the plane of the other. This motion still permits an overlap of the S lone pair of one unit with the σ^*(SC) orbital of the other, as illustrated in Figure 6a. As in coplanar dimer **e**, **d** also contains a secondary charge transfer to augment the interaction. The source of the density for this complementary interaction is the π-orbital of S, which is partially a lone pair as it is poorly integrated into the π-system of the ring. The overlap of the orbitals involved is portrayed in Figure 6b, for which $E(2)$ is comparable to that involving the σ

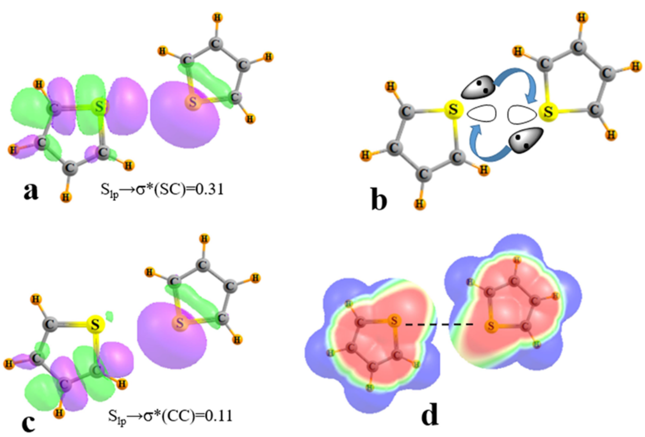

Figure 5. Alignment between the S lone pair of one monomer and (a) σ^*(CS) and (c) σ^*(CC) antibonding orbitals of its partner in structure **e**. Purple and green colors indicate opposite phases of the wave function. NBO $E(2)$ values reported in kcal/mol. (b) Cartoon showing dual transfer in both directions. (d) Disposition of MEP of two monomers. Blue and red colors, respectively, indicate +13 and −13 kcal/mol.

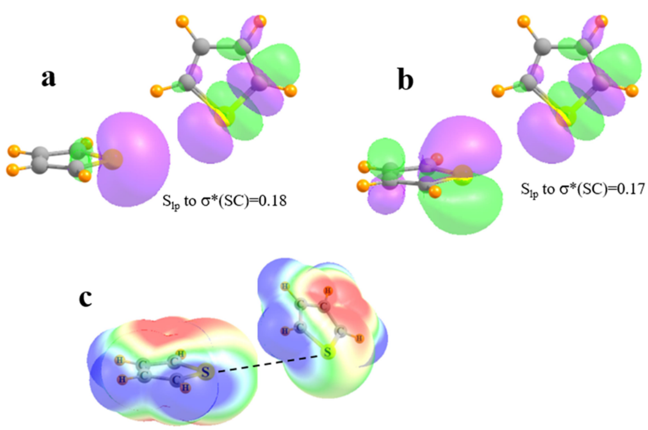

Figure 6. Alignment between the σ^*(SC) antibonding orbital of one monomer and (a) S σ-lone pair and (b) S π-lone pair of its partner in structure **d**. Purple and green colors indicate opposite phases of the wave function. NBO $E(2)$ values reported in kcal/mol. (c) Disposition of MEP of two monomers where blue and red colors, respectively, indicate +13 and −13 kcal/mol.

https://doi.org/10.1021/acs.jpca.2c02451
J. Phys. Chem. A 2022, 126, 4025−4035

lone pair of S in Figure 6a. (Like **e**, the symmetry of **d** also leads to a doubling of these quantities, as charge transfers in the reverse direction are also present.)

With regard to the electrostatics, it might be noted from Figure 2b that the MEP becomes less positive as the point of reference leaves the molecular plane. The displacement of the two molecules that occurs within structure **d** capitalizes on this behavior, which will tend to reduce any repulsive electrostatic force between the two Y atoms. The MEPs of the two monomers are placed in their appropriate positions of the **d** dimer in Figure 6c and illustrate how the displacement of one molecule out of the plane of the other minimizes any contacts between positive blue areas. It is in part due to this rearrangement that the ES term is more negative for **d** than for **e**.

Other insights into the nature of the bonding can be achieved by switching out one of the H atoms of SC_4H_4 with an F atom. A planar structure very closely akin to dimer **e** was optimized although the two CH···S HBs that help stabilize the thiophene dimer are no longer possible. The absence of these HBs accounts for the weakening of the total interaction, with E_{int} cut from 2.26 to 1.02 kcal/mol, and the R(S···S) distance expanded from 3.478 to 3.502 Å. One might thus approximate this 1 kcal/mol quantity as a reasonable estimate as to the S···S chalcogen bond strength when in this coplanar configuration. This value is quite similar to a computation[73] at the much higher CCSD(T) level with a complete basis set extrapolation. The monosubstituted SC_4H_3F dimer also engages in a perpendicular structure like that of **b**, which is primarily stabilized by a S···π ChB. The interaction energy of this dimer is 3.59 kcal/mol, which is slightly larger than 2.66 kcal/mol in its unsubstituted analogue. The added stability can be attributed in part to a pair of weak halogen bonds (F···F and F···S) that complement the ChB. Another variation might be to change one of the CH groups adjacent to Y to a N atom. Just as in the case of the CH → CF substitution, the homodimer of SNC_3H_3 forms a coplanar structure much like **e**. Also lacking the CH···N HBs of **e**, the interaction energy of this dimer is only 1.02 kcal/mol.

■ DISCUSSION

It is of some interest to summarize the types of noncovalent bonds involved in each class of geometry and to study how these bond types impact the overall stability. All of the homodimers examined here are of moderate strength, with binding energies in the range between 1.5 and 4.6 kcal/mol. Even though the MEP is most positive in the regions surrounding the H atoms, perpendicular structure **c**, which is bound almost entirely by several HBs, is not the most strongly bound. It is surpassed by geometry **b**, which is stabilized primarily by a Y···π ChB, without the aid of auxiliary noncovalent bonds. The interaction energies of these structures provide the best unvarnished view of the strength of the ChB in isolation from other bonds. As such, these ChBs vary from 2.7 kcal/mol for S, up to 4.3 kcal/mol for Te, with Se in between. This trend obeys normal expectations for ChBs. The optimal binding choice, global minimum **a**, involves a combination of HBs with a Y···π ChB, and these HBs add a little less than 1 kcal/mol to the interaction energy.

The monomer arrangements of slipped parallel **d** and planar **e** are unable to present a simple interaction of an extensive positive MEP of one unit with a negative MEP of the other, as is possible for the T-structures. They nevertheless adopt geometries that minimize any Coulombic repulsion to the point that the overall electrostatic interaction is slightly negative. Slipped parallel **d** is better able to minimize Coulombic repulsions and so is somewhat more stable than planar **e**. The ChBs in these two structures are of the Y···Y type where charge is transferred from the lone pair of one atom to the σ^*(YC) orbital of its partner. However, the symmetry is such that there is an equal transfer in the opposite direction, essentially doubling the stabilizing influence of the Y···Y ChB. Rather than the CH···π HBs of the perpendicular structures, the auxiliary bonds in **d** and **e** are of CH···Y type and appear to be important for the formation of these classes of dimers, which cannot depend entirely upon a ChB. As such, the **d** conformations tend to be more stable than the perpendicular **c**, which is bound almost exclusively by a π ChB. The diminishing electronegativity from S to Te progressively weakens these auxiliary bonds. Consequently, the interaction energy of the **e** dimer of Se is smaller than that of S, and this geometry disappears entirely from the surface of Te.

As indicated above, the interactions examined here are not necessarily pure ChBs but combine them with other sorts of bonds such as CH···Y and CH···π. Hence, it is of interest to compare these interactions with a purer form of ChB. The combination of several CH···π HBs, which is the dominant factor in complex **c**, leads to a total interaction energy of 1.39 for Y = Se, which is considerably smaller than an FH···π energy of 5.11 kcal/mol in Figure 3c. This disparity is sensible in light of the much stronger ability of FH to donate a proton. If the CH group of SeC_4H_4 is combined with NH_3 as the base, the interaction energy of this pure CH···N HB is 1.57 kcal/mol (see Figure 3b), so one can consider the π-system of SeC_4H_4 as comparable to NH_3 in terms of electron donation. This same NH_3 base engages in a joint ChB/HB with SeC_4H_4 (Figure 3a) with a combined strength of 3.17 kcal/mol. This quantity is only slightly stronger than the Se···Se ChB of dimer **e**, which has no apparent augmenting HB, so it seems that the Se of the ring is comparable to NH_3 as a ChB partner.

It is perhaps surprising that chalcogen bonds can be formed between molecules without a positively charged σ or even π-hole. However, as mentioned above, the absence of such a hole does not necessarily preclude a stabilizing interaction, as other factors can compensate. In addition, this idea has been manifested in the past. For example, a series of calculations[74] have documented the ability of a molecule like $H_2T = Y$, where T represents any of a group of tetrel atoms, to engage in a ChB with a N-base despite a σ-hole of negative sign. Murray and Politzer[75] have compiled a longer list of stable complexes forming despite a negative σ-hole in the context of halogen bonds, work that was seconded by Wang et al.[76] for another series of complexes.

Earlier comparisons between experiments and computations[77] have emphasized the importance of orbital delocalization, aka induction, in the chalcogen bonds involving thiophene and selenophenes. The authors noted charge transfer between the same orbitals as noted above. This conclusion is also in line with the observation here that IND typically outweighs ES in the homodimers. Another recent study[78] has experimentally verified the ability of tellurophenes to participate in chalcogen bonds, in this case with anions such as chloride, bromide, nitrate, benzoate, and toluensulfonate. There are instances of bipodal bonding involving two such Te atoms and a single anion. Other work[79] furthered the study of chalcogen bonding by thiophene, selenophene, and tellurophene as a means of binding anions. It was found that these chalcogen bonds can be overshadowed by H-bonds for S and Se but that it is the ChB that dominates for Te. This trend is consistent with the higher relative energy of the H-bonded conformer **c** for Te, as compared to S and Se.

https://doi.org/10.1021/acs.jpca.2c02451
J. Phys. Chem. A 2022, 126, 4025−4035

Earlier calculations have provided parameters regarding native chalcogen bond strengths. In the context of the NH_3 base, RMeS···NH_3 interaction energies lie in the range between 2.3 and 4.4 kcal/mol, depending upon the nature of R.[80] When the lone pair of NH_3 is replaced by a C═C π-system[53] as in ethylene or butadiene, the ensuing S···π ChB strength varies between 4 and 7 kcal/mol, with dispersion making a contribution comparable to electrostatics. The bond is strengthened by polyfluorination, as in SF_4, whose interaction energy with NH_3 is 6.6 kcal/mol.[52] Similar patterns apply to Se: interaction energies of R_2Se with NH_3 range up to as much as 10 kcal/mol for FHSe.[81]

A detailed survey of the entire gamut of crystal structures involving thiophene and related units of the sort studied here is beyond the scope of this paper. Moreover, the emphasis here lies with the intrinsic preferences for geometrical alignment, free of external forces such as crystal packing phenomena. Nonetheless, there are indications that perpendicular alignments of the sort representing the most stable dimers **a**, **b**, and **c**, as well as certain others, do appear in crystals,[49,82−89] albeit modified a bit by crystal packing forces. In a broader sense, earlier surveys of crystal structures[33] had suggested a proclivity of nucleophiles to approach a divalent S either from directly above or within the molecular plane, consistent with the perpendicular and coplanar dimers elucidated here.

For a wider perspective, one may relate the ChBs studied here with comparable halogen bonds (XBs). Homodimers of the type R-X···X-R (X = halogen) prefer to adopt a geometry wherein one θ(RX···X) angle is nearly linear and the other roughly 90°. This so-called Type II arrangement allows the σ^*(RX) orbital of one unit to best align with one of the lone pairs on the electron-donating X of its partner. An alternative structure, referred to as Type I, is symmetric in the sense that the two θ(RX···X) angles are roughly equal to one another.[90−92] This geometry is less stable than Type II, and various reasons have been advanced for this difference over the years.[90,93−97] Recent calculations[98] have shown that Type I represents a transition state for the interconversion of one Type II structure into the other, with the two RX molecules reversing roles as an electron donor or acceptor. The binding of Type I rests on a pair of bent halogen bonds, rather than the single linear XB of Type II.

Structure **e** of the YC_4H_4 dimers contains the primary feature of a Type I halogen bonded pair, as does **d** to some extent. These configurations are symmetric and rely for their stability on a pair of Y···Y ChBs, each of them bent as displayed in Figures 5 and 6. In contrast to RX dimers, there was no minimum identified on the surfaces of these YC_4H_4 dimers containing a single linear ChB. Attempts to identify a configuration of this sort, using an appropriate structure as a starting point for the optimization, failed as the dimer reverted to one of the geometries described above. One can force the dimer into this sort of Type II geometry, by restricting a CY bond of one unit to line up with the Y lone pair of the partner. The resulting configuration, containing a single linear ChB, is higher in energy than the coplanar dimer **e**. Using thiophene as an example, this structure is less stable than **e** by 0.6 kcal/mol, and R(S···S) is longer by 0.084 Å. Hence, it would appear that there is a reversal of sorts between halogen and chalcogen bonds. While a single linear XB is preferred over a pair of bent XBs, the opposite is true of ChBs where it is the pair of bent bonds that is preferred. What is common in both cases, however, is that there is only a small difference in energy between these two sorts of bonding scenarios. One possible explanation for the absence of dimer **e** for Te might have to do with its larger size and the greater exchange repulsion between a pair of Te atoms that might result.

The fairly similar energies of the Type I and II geometries in both the ChB systems presented here, and in the XBs discussed previously, lead to the hypothesis that perhaps this might be a common theme in noncovalent bonds. The near equivalence of a single linear bond on the one hand and a pair of weaker bent bonds on the other may be a general characteristic that will become apparent as future work materializes.

It is noted finally that there are small changes in the data from one chalcogen atom to the next, e.g., energetics, AIM parameters, and geometric details. For example, the interaction energies tend to rise with larger Y atoms, as do the intermolecular distances. What is most important, though, are the strong similarities between the behavior of the homodimers of thiophene, selenophene, and tellurophene.

■ CONCLUSIONS

The homodimers of YC_4H_4 adopt two general categories of geometry. There are three perpendicular dimer types where one unit approaches the other from above its molecular plane in a T-shape. These complexes are held together by some combination of Y···π chalcogen and CH···π H-bonds. These T-shapes are further stabilized by the juxtaposition of the positive MEP in the plane of one molecule with the negative region above the plane of the other. Another category, and somewhat less stable, is a sort of slipped parallel geometry combining a Y···Y ChB with interactions between the CH groups of the two molecules. Last is a coplanar dimer, composed chiefly of a Y···Y ChB. The ChBs in the latter two structures are ″duplex″ in the sense that each Y atom serves as both an electron donor and acceptor. The interaction energies of these dimers range from 1.6 up to 4.6 kcal/mol. Those complexes, held together in large part by a ChB, obey the standard pattern where the bond strengthens as the Y atom grows larger. A simple examination of the MEPs of the two units would not necessarily predict the stability of the two latter geometries, although they do in fact benefit from a Coulombic attraction.

■ ASSOCIATED CONTENT

Supporting Information

The Supporting Information is available free of charge at https://pubs.acs.org/doi/10.1021/acs.jpca.2c02451.

Molecular geometries, AIM and NCI diagrams contained therein, as well as density, ELF, and MEP diagrams of thiophene and tellurophene; cartesian coordinates and comparison of energetics at different levels of theory (PDF)

■ AUTHOR INFORMATION

Corresponding Author

Steve Scheiner − *Department of Chemistry and Biochemistry, Utah State University, Logan, Utah 84322-0300, United States*; orcid.org/0000-0003-0793-0369; Email: steve.scheiner@usu.edu

Complete contact information is available at: https://pubs.acs.org/10.1021/acs.jpca.2c02451

Notes

The author declares no competing financial interest.

https://doi.org/10.1021/acs.jpca.2c02451
J. Phys. Chem. A 2022, 126, 4025−4035

■ ACKNOWLEDGMENTS

This material was based upon work supported by the National Science Foundation under Grant No. 1954310.

■ REFERENCES

(1) Schuster, P.; Zundel, G.; Sandorfy, C. *The Hydrogen Bond. Recent Developments in Theory and Experiments*; North-Holland Publishing Co.: Amsterdam, 1976.
(2) Hobza, P.; Zahradník, R. Van der Waals molecules: Quantum chemistry, physical properties, and reactivity. *Int. J. Quantum Chem.* **1983**, *23*, 325−338.
(3) Brobjer, J. T.; Murrell, J. N. Geometries of van der Waals complexes of small polar molecules. *J. Chem. Soc., Faraday Trans. 2* **1983**, *79*, 1455−1464.
(4) Xie, Y.; Remington, R. B.; Schaefer, H. F., III The protonated water dimer: Extensive theoretical studies of $H_5O_2^+$. *J. Chem. Phys.* **1994**, *101*, 4878−4884.
(5) Scheiner, S.; Szczęśniak, M. M.; Bigham, L. D. Ab initio study of proton transfers including effects of electron correlation. *Int. J. Quantum Chem.* **1983**, *23*, 739−751.
(6) Pearcy, A. C.; Mason, K. A.; El-Shall, M. S. Ionic Hydrogen and Halogen Bonding in the Gas Phase Association of Acetonitrile and Acetone with Halogenated Benzene Cations. *J. Phys. Chem. A* **2019**, *123*, 1363−1371.
(7) Hillenbrand, E. A.; Scheiner, S. Effects of molecular charge and methyl substitution on proton transfers between oxygen atoms. *J. Am. Chem. Soc.* **1984**, *106*, 6266−6273.
(8) Szcześniak, M. M.; Scheiner, S. Møller-Plesset treatment of electron correlation in $(HOHOH)^-$. *J. Chem. Phys.* **1982**, *77*, 4586−4593.
(9) Scheiner, S.; Duan, X. Effect of intermolecular orientation upon proton transfer within a polarizable medium. *Phys. Chem. Chem. Phys.* **1991**, *60*, 874−883.
(10) Cybulski, S. M.; Scheiner, S. Hydrogen bonding and proton transfers involving the carboxylate group. *J. Am. Chem. Soc.* **1989**, *111*, 23−31.
(11) Gilli, G.; Gilli, P. *The Nature of the Hydrogen Bond*; Oxford University Press: Oxford, UK, 2009.
(12) Jeffrey, G. A.; Saenger, W. *Hydrogen Bonding in Biological Structures*; Springer-Verlag: Berlin, 1991.
(13) Scheiner, S.; Kleier, D. A.; Lipscomb, W. N. Molecular orbital studies of enzyme activity: I: Charge relay system and tetrahedral intermediate in acylation of serine proteinases. *Proc. Natl. Acad. Sci. U. S. A.* **1975**, *72*, 2606−2610.
(14) Cybulski, S. M.; Scheiner, S. Hydrogen bonding and proton transfers involving triply bonded atoms. HC≡N and HC≡CH. *J. Am. Chem. Soc.* **1987**, *109*, 4199−4206.
(15) Alkorta, I.; Sánchez-Sanz, G.; Elguero, J.; Del Bene, J. E. Influence of hydrogen bonds on the P···P pnicogen bond. *J. Chem. Theory Comput.* **2012**, *8*, 2320−2327.
(16) Bauzá, A.; Mooibroek, T. J.; Frontera, A. σ-Hole Opposite to a Lone Pair: Unconventional Pnicogen Bonding Interactions between ZF_3 (Z=N, P, As, and Sb) Compounds and Several Donors. *ChemPhysChem* **2016**, *17*, 1608−1614.
(17) Latajka, Z.; Scheiner, S. The potential energy surface of $(NH_3)_2$. *J. Chem. Phys.* **1986**, *84*, 341−347.
(18) Mertsalov, D. F.; Gomila, R. M.; Zaytsev, V. P.; Grigoriev, M. S.; Nikitina, E. V.; Zubkov, F. I.; Frontera, A. On the Importance of Halogen Bonding Interactions in Two X-ray Structures Containing All Four (F, Cl, Br, I) Halogen Atoms. *Crystals* **2021**, *11*, 1406.
(19) Grabowski, S. J. Hydrogen and halogen bonds are ruled by the same mechanisms. *Phys. Chem. Chem. Phys.* **2013**, *15*, 7249−7259.
(20) Kumar, V.; Scilabra, P.; Politzer, P.; Terraneo, G.; Daolio, A.; Fernandez-Palacio, F.; Murray, J. S.; Resnati, G. Tetrel and Pnictogen Bonds Complement Hydrogen and Halogen Bonds in Framing the Interactional Landscape of Barbituric Acids. *Cryst. Growth Des.* **2021**, *21*, 642−652.
(21) Liu, N.; Li, Q.; McDowell, S. A. C. Reliable Comparison of Pnicogen, Chalcogen, and Halogen Bonds in Complexes of 6-OXF_2-Fulvene (X = As, Sb, Se, Te, Be, I) With Three Electron Donors. *Front. Chem.* **2020**, *8*, No. 608486.
(22) Nziko, V. d. P. N.; Scheiner, S. Comparison of π-hole tetrel bonding with σ-hole halogen bonds in complexes of XCN (X = F, Cl, Br, I) and NH_3. *Phys. Chem. Chem. Phys.* **2016**, *18*, 3581−3590.
(23) Gleiter, R.; Werz, D. B.; Rausch, B. J. A World Beyond Hydrogen Bonds?—Chalcogen−Chalcogen Interactions Yielding Tubular Structures. *Chem. − Eur. J.* **2003**, *9*, 2676−2683.
(24) Biswal, H. S.; Sahu, A. K.; Galmés, B.; Frontera, A.; Chopra, D. Se···O/S and S···O Chalcogen Bonds in Small Molecules and Proteins: A Combined CSD and PDB Study. *ChemBioChem* **2022**, *23*, No. e202100498.
(25) Frontera, A.; Bauzá, A. On the Importance of σ−Hole Interactions in Crystal Structures. *Crystals* **2021**, *11*, 1205.
(26) Carugo, O.; Resnati, G.; Metrangolo, P. Chalcogen Bonds Involving Selenium in Protein Structures. *ACS Chem. Biol.* **2021**, *16*, 1622−1627.
(27) Scheiner, S. Participation of S and Se in hydrogen and chalcogen bonds. *CrystEngComm* **2021**, *23*, 6821−6837.
(28) Fernández Riveras, J. A.; Frontera, A.; Bauzá, A. Selenium chalcogen bonds are involved in protein−carbohydrate recognition: a combined PDB and theoretical study. *Phys. Chem. Chem. Phys.* **2021**, *23*, 17656−17662.
(29) Scheiner, S. Highly Selective Halide Receptors Based on Chalcogen, Pnicogen, and Tetrel Bonds. *Chem. − Eur. J.* **2016**, *22*, 18850−18858.
(30) Dhaka, A.; Jeannin, O.; Aubert, E.; Espinosa, E.; Fourmigué, M. Chalcogen Bonding in Co-Crystals: Activation through 1,4-Perfluorophenylene vs. 4,4′-Perfluorobiphenylene Cores. *Molecules* **2021**, *26*, 4050.
(31) Echeverría, J. Cooperative Effects between Hydrogen Bonds and C═O···S Interactions in the Crystal Structures of Sulfoxides. *Cryst. Growth Des.* **2021**, *21*, 2481−2487.
(32) Fick, R. J.; Kroner, G. M.; Nepal, B.; Magnani, R.; Horowitz, S.; Houtz, R. L.; Scheiner, S.; Trievel, R. C. Sulfur−Oxygen Chalcogen Bonding Mediates AdoMet Recognition in the Lysine Methyltransferase SET7/9. *ACS Chem. Biol.* **2016**, *11*, 748−754.
(33) Desiraju, G. R.; Nalini, V. Database analysis of crystal-structure-determining interactions involving sulphur: implications for the design of organic metals. *J. Mater. Chem.* **1991**, *1*, 201−203.
(34) Burling, F. T.; Goldstein, B. M. Computational studies of nonbonded sulfur-oxygen and selenium-oxygen interactions in the thiazole and selenazole nucleosides. *J. Am. Chem. Soc.* **1992**, *114*, 2313−2320.
(35) Nagao, Y.; Hirata, T.; Goto, S.; Sano, S.; Kakehi, A.; Iizuka, K.; Shiro, M. Intramolecular nonbonded S···O interaction recognized in (acylimino)thiadiazoline derivatives as angiotensin II receptor antagonists and related compounds. *J. Am. Chem. Soc.* **1998**, *120*, 3104−3110.
(36) Iwaoka, M.; Takemoto, S.; Tomoda, S. Statistical and theoretical investigations on the directionality of nonbonded S···O interactions. Implications for molecular design and protein engineering. *J. Am. Chem. Soc.* **2002**, *124*, 10613−10620.
(37) Iwaoka, M.; Takemoto, S.; Okada, M.; Tomoda, S. Weak nonbonded S···X (X = O, N, and S) interactions in proteins. statistical and theoretical studies. *Bull. Chem. Soc. Jpn.* **2002**, *75*, 1611−1625.
(38) Sanz, P.; Mó, O.; Yáñez, M. Characterization of intramolecular hydrogen bonds and competitive chalcogen−chalcogen interactions on the basis of the topology of the charge density. *Phys. Chem. Chem. Phys.* **2003**, *5*, 2942−2947.
(39) Sanz, P.; Yáñez, M.; Mó, O. Resonance-assisted intramolecular chalcogen−chalcogen interactions? *Chem. − Eur. J.* **2003**, *9*, 4548−4555.
(40) Politzer, P.; Murray, J. S.; Lane, P. σ-Hole bonding and hydrogen bonding: Competitive interactions. *Int. J. Quantum Chem.* **2007**, *107*, 3046−3052.

(41) Bleiholder, C.; Gleiter, R.; Werz, D. B.; Köppel, H. Theoretical investigations on heteronuclear chalcogen-chalcogen interactions: On the nature of weak bonds between chalcogen centers. *Inorg. Chem.* **2007**, *46*, 2249−2260.
(42) Cozzolino, A. F.; Vargas-Baca, I. The supramolecular chemistry of 1,2,5-chalcogenadiazoles. *J. Organomet. Chem.* **2007**, *692*, 2654−2657.
(43) Junming, L.; Yunxiang, L.; Subin, Y.; Weiliang, Z. Theoretical and crystallographic data investigations of noncovalent S···O interactions. *Struct. Chem.* **2011**, *22*, 757−763.
(44) Dhaka, A.; Jeannin, O.; Aubert, E.; Espinosa, E.; Fourmigué, M. Supramolecular rectangles through directional chalcogen bonding. *Chem. Commun.* **2021**, *57*, 4560−4563.
(45) Cozzolino, A. F.; Dimopoulos-Italiano, G.; Lee, L. M.; Vargas-Baca, I. Chalcogen−Nitrogen Secondary Bonding Interactions in the Gas Phase − Spectrometric Detection of Ionized Benzo-2,1,3-telluradiazole Dimers. *Eur. J. Inorg. Chem.* **2013**, *2013*, 2751−2756.
(46) Kumar, V.; Xu, Y.; Bryce, D. L. Double Chalcogen Bonds: Crystal Engineering Stratagems via Diffraction and Multinuclear Solid-State Magnetic Resonance Spectroscopy. *Chem. − Eur. J.* **2020**, *26*, 3275−3286.
(47) Wen, C.; Shi, Y.; Lu, Y.; Xu, Z.; Liu, H. 2Ch−2N Square Chalcogen Bonds between Pairs of Radicals: A Case Study of 1,2,3,5-Dichalcogenadiazolyl Derivatives. *J. Phys. Chem. A* **2021**, *125*, 8572−8580.
(48) Liang, J.; Shi, Y.; Lu, Y.; Xu, Z.; Liu, H. Square tetravalent chalcogen bonds in dimeric aggregates: a joint crystallographic survey and theoretical study. *CrystEngComm* **2022**, *24*, 975−986.
(49) Scilabra, P.; Terraneo, G.; Resnati, G. The Chalcogen Bond in Crystalline Solids: A World Parallel to Halogen Bond. *Acc. Chem. Res.* **2019**, *52*, 1313−1324.
(50) Zierkiewicz, W.; Wysokiński, R.; Michalczyk, M.; Scheiner, S. Chalcogen bonding of two ligands to hypervalent YF_4 (Y = S, Se, Te, Po). *Phys. Chem. Chem. Phys.* **2019**, *21*, 20829−20839.
(51) Iwaoka, M.; Isozumi, N. Hypervalent nonbonded interactions of a divalent sulfur atom. Implications in protein architecture and the functions. *Molecules* **2012**, *17*, 7266−7283.
(52) Nziko, V. d. P. N.; Scheiner, S. Chalcogen Bonding between Tetravalent SF_4 and Amines. *J. Phys. Chem. A* **2014**, *118*, 10849−10856.
(53) Nziko, V. d. P. N.; Scheiner, S. S···π Chalcogen Bonds between SF_2 or SF_4 and C−C Multiple Bonds. *J. Phys. Chem. A* **2015**, *119*, 5889−5897.
(54) Scheiner, S.; Lu, J. Halogen, Chalcogen, and Pnicogen Bonding Involving Hypervalent Atoms. *Chem. − Eur. J.* **2018**, *24*, 8167−8177.
(55) Fringuelli, F.; Marino, G.; Taticchi, A.; Grandolini, G. A comparative study of the aromatic character of furan, thiophen, selenophen, and tellurophen. *J. Chem. Soc. Perkin Trans. 2* **1974**, *2*, 332−337.
(56) Frisch, M. J.; Trucks, G. W.; Schlegel, H. B.; Scuseria, G. E.; Robb, M. A.; Cheeseman, J. R.; Scalmani, G.; Barone, V.; Petersson, G. A.; Nakatsuji, H.; Li, X.; Caricato, M.; Marenich, A. V.; Bloino, J.; Janesko, B. G.; Gomperts, R.; Mennucci, B.; Hratchian, H. P.; Ortiz, J. V.; Izmaylov, A. F.; Sonnenberg, J. L.; Williams-Young, D.; Ding, F.; Lipparini, F.; Egidi, F.; Goings, J.; Peng, B.; Petrone, A.; Henderson, T.; Ranasinghe, D.; Zakrzewski, V. G.; Gao, J.; Rega, N.; Zheng, G.; Liang, W.; Hada, M.; Ehara, M.; Toyota, K.; Fukuda, R.; Hasegawa, J.; Ishida, M.; Nakajima, T.; Honda, Y.; Kitao, O.; Nakai, H.; Vreven, T.; Throssell, K.; Montgomery, J. A., Jr.; Peralta, J. E.; Ogliaro, F.; Bearpark, M. J.; Heyd, J. J.; Brothers, E. N.; Kudin, K. N.; Staroverov, V. N.; Keith, T. A.; Kobayashi, R.; Normand, J.; Raghavachari, K.; Rendell, A. P.; Burant, J. C.; Iyengar, S. S.; Tomasi, J.; Cossi, M.; Millam, J. M.; Klene, M.; Adamo, C.; Cammi, R.; Ochterski, J. W.; Martin, R. L.; Morokuma, K.; Farkas, O.; Foresman, J. B.; Fox, D. J. *Gaussian 16 Rev. C.01*, Wallingford, CT, 2016.
(57) Zhao, Y.; Truhlar, D. G. The M06 suite of density functionals for main group thermochemistry, thermochemical kinetics, noncovalent interactions, excited states, and transition elements: two new functionals and systematic testing of four M06-class functionals and 12 other functionals. *Theor. Chem. Acc.* **2008**, *120*, 215−241.
(58) Wang, R.; Lu, Y.; Xu, Z.; Liu, H. Triangular Interchalcogen Interactions: A Joint Crystallographic Data Analysis and Theoretical Study. *J. Phys. Chem. A* **2021**, *125*, 4173−4183.
(59) Devore, D. P.; Ellington, T. L.; Shuford, K. L. Interrogating the Interplay between Hydrogen and Halogen Bonding in Graphitic Carbon Nitride Building Blocks. *J. Phys. Chem. A* **2020**, *124*, 10817−10825.
(60) Zhao, Q. Mutual influence of tetrel and halogen bonds between XCN (X=Cl, Br) and 4-TF_3-pyridine (T=C, Si, Ge). *J. Mol. Model.* **2020**, *26*, 329.
(61) Yang, J.; Yu, Q.; Yang, F.-L.; Lu, K.; Yan, C.-X.; Dou, W.; Yang, L.; Zhou, P.-P. Competition and cooperativity of hydrogen-bonding and tetrel-bonding interactions involving triethylene diamine (DABCO), H_2O and CO_2 in air. *New J. Chem.* **2020**, *44*, 2328−2338.
(62) Schuchardt, K. L.; Didier, B. T.; Elsethagen, T.; Sun, L.; Gurumoorthi, V.; Chase, J.; Li, J.; Windus, T. L. Basis Set Exchange: A Community Database for Computational Sciences. *J. Chem. Inf. Model.* **2007**, *47*, 1045−1052.
(63) Boys, S. F.; Bernardi, F. The calculation of small molecular interactions by the differences of separate total energies. Some procedures with reduced errors. *Mol. Phys.* **1970**, *19*, 553−566.
(64) Lu, T.; Chen, F. Multiwfn: A multifunctional wavefunction analyzer. *J. Comput. Chem.* **2012**, *33*, 580−592.
(65) Keith, T. A. *AIMAll*; TK Gristmill Software: Overland Park KS, 2013.
(66) Reed, A. E.; Weinstock, R. B.; Weinhold, F. Natural population analysis. *J. Chem. Phys.* **1985**, *83*, 735−746.
(67) Reed, A. E.; Curtiss, L. A.; Weinhold, F. Intermolecular interactions from a natural bond orbital, donor-acceptor viewpoint. *Chem. Rev.* **1988**, *88*, 899−926.
(68) Jeziorski, B.; Moszynski, R.; Szalewicz, K. Perturbation Theory Approach to Intermolecular Potential Energy Surfaces of van der Waals Complexes. *Chem. Rev.* **1994**, *94*, 1887−1930.
(69) Szalewicz, K.; Jeziorski, B. In *Molecular Interactions. From Van der Waals to Strongly Bound Complexes*, Scheiner, S., Ed.; Wiley: New York, 1997; 3−43.
(70) Werner, H.-J.; Knowles, P. J.; Manby, F. R.; Schütz, M.; Celani, P.; Knizia, G.; Korona, T.; Lindh, R.; Mitrushenkov, A.; Rauhut, G.; Shamasundar, K.R.; Adler, T. B.; Amos, R. D.; Bernhardsson, A.; Berning, A.; Cooper, D. L.; Deegan, M. J. O.; Dobbyn, A. J.; Eckert, F.; Goll, E.; Hampel, C.; Hesselmann, A.; Hetzer, G.; Hrenar, T.; Jansen, G.; Köppl, C.; Liu, Y.; Lloyd, A. W.; Mata, R. A.; May, A. J.; McNicholas, S. J.; Meyer, W.; Mura, M. E.; Nicklass, A.; O'Neill, D. P.; Palmieri, P.; Peng, D.; Pflüger, K.; Pitzer, R.; Reiher, M.; Shiozaki, T.; Stoll, H.; Stone, A. J.; Tarroni, R.; Thorsteinsson, T.; Wang, M. *MOLPRO, Version 2006*; 2010.
(71) Alvarez, S. A cartography of the van der Waals territories. *Dalton Trans.* **2013**, *42*, 8617−8636.
(72) Mehta, N.; Fellowes, T.; White, J. M.; Goerigk, L. CHAL336 Benchmark Set: How Well Do Quantum-Chemical Methods Describe Chalcogen-Bonding Interactions? *J. Chem. Theory Comput.* **2021**, *17*, 2783−2806.
(73) Zhang, Y.; Wang, W. The Bifurcated sigma-Hole...sigma-Hole Stacking Interactions. *Molecules* **2022**, *27*, 1252.
(74) Wysokiński, R.; Zierkiewicz, W.; Michalczyk, M.; Scheiner, S. Ability of Lewis Acids with Shallow σ-Holes to Engage in Chalcogen Bonds in Different Environments. *Molecules* **2021**, *26*, 6394.
(75) Murray, J. S.; Politzer, P. Can Counter-Intuitive Halogen Bonding Be Coulombic? *ChemPhysChem* **2021**, *22*, 1201−1207.
(76) Wang, R.; Li, Q.; Scheiner, S. Complexes of HArF and AuX (X = F, Cl, Br, I). Comparison of H-bonds, halogen bonds, F-shared bonds and covalent bonds. *Appl. Organomet. Chem.* **2020**, *34*, No. e5891.
(77) Pascoe, D. J.; Ling, K. B.; Cockroft, S. L. The Origin of Chalcogen-Bonding Interactions. *J. Am. Chem. Soc.* **2017**, *139*, 15160−15167.
(78) Garrett, G. E.; Carrera, E. I.; Seferos, D. S.; Taylor, M. S. Anion recognition by a bidentate chalcogen bond donor. *Chem. Commun.* **2016**, *52*, 9881−9884.

(79) Navarro-García, E.; Galmés, B.; Velasco, M. D.; Frontera, A.; Caballero, A. Anion Recognition by Neutral Chalcogen Bonding Receptors: Experimental and Theoretical Investigations. *Chem. − Eur. J.* **2020**, *26*, 4706−4713.

(80) Adhikari, U.; Scheiner, S. Effects of Charge and Substituent on the S···N Chalcogen Bond. *J. Phys. Chem. A* **2014**, *118*, 3183−3192.

(81) Dong, W.; Li, Q.; Scheiner, S. Comparative Strengths of Tetrel, Pnicogen, Chalcogen, and Halogen Bonds and Contributing Factors. *Molecules* **2018**, *23*, 1681.

(82) Luz, E. Q.; Santana, F. S.; Silverio, G. L.; Tullio, S. C. M. C.; Iodice, B.; Prola, L. D. T.; Barbosa, R. V.; Rampon, D. S. Crystal structures of 3-halo-2-organochalcogenylbenzo[b]chalcogenophenes. *Acta Crystallogr. E Crystallogr. Commun.* **2022**, *78*, 275−281.

(83) Xu, W.; Wu, L.; Fang, M.; Ma, Z.; Shan, Z.; Li, C.; Wang, H. Diseleno[2,3-b:3′,2′-d]selenophene and Diseleno[2,3-b:3′,2′-d] thiophene: Building Blocks for the Construction of [7]Helicenes. *J. Org. Chem.* **2017**, *82*, 11192−11197.

(84) Das, S.; Bedi, A.; Krishna, G. R.; Reddy, C. M.; Zade, S. S. Cyclopenta[c]selenophene based cooligomers and their polymers: comparative study with thiophene analogues. *Org. Biomol. Chem.* **2011**, *9*, 6963−6972.

(85) Helmholdt, R. B.; Sonneveld, E. J.; Vande Velde, C. M. L.; Blockhuys, F.; Lenstra, A. T. H.; Geise, H. J.; Peschar, R. Structures of tetrabromothiophene and tetrabromoselenophene: the influence of the heteroatom on the heterophene packing. *Acta Crystallogr. B* **2007**, *63*, 783−790.

(86) Ragusa, A. C.; Peloquin, A. J.; McMillen, C. D.; Pennington, W. T. 2,5-Diiodothiophene: A Versatile Halogen Bonding Synthon for Crystal Engineering. *Cryst. Growth Des.* **2022**, *22*, 1906−1913.

(87) Takimiya, K.; Usui, S.; Sato, A.; Kanazawa, K.; Kawabata, K. Packing structures of (trialkylsilyl)ethynyl-substituted dinaphtho[2,3-b:2′,3′-f]thieno[3,2-b]thiophenes (DNTTs): effects of substituents on crystal structures and transport properties. *J. Mater. Chem. C Mater.* **2022**, *10*, 2775−2782.

(88) Yoshida, R.; Tachikawa, T.; Ito, S. Mechano- and Thermo-responsive Luminescence of Crystalline Thienylbenzothiadiazole Derivatives: Stepwise Hypsochromic Switching of Near-Infrared Emission. *Cryst. Growth Des.* **2022**, *22*, 547−558.

(89) Xie, P.; Liu, T.; Sun, J.; Yang, J. Structures, Properties, and Device Applications for [1]Benzothieno[3,2-b]Benzothiophene Derivatives. *Adv. Funct. Mater.* **2022**, *32*, No. 2200843.

(90) Desiraju, G. R.; Parthasarathy, R. The nature of halogen....halogen interactions: are short halogen contacts due to specific attractive forces or due to close packing of nonspherical atoms? *J. Am. Chem. Soc.* **1989**, *111*, 8725−8726.

(91) Pedireddi, V. R.; Reddy, D. S.; Goud, B. S.; Craig, D. C.; Rae, A. D.; Desiraju, G. R. The nature of halogen ··· halogen interactions and the crystal structure of 1,3,5,7-tetraiodoadamantane. *J. Chem. Soc. Perkin Trans. 2* **1994**, *2*, 2353−2360.

(92) Fourmigué, M. Halogen bonding: Recent advances. *Curr. Opin. Solid State Mater. Sci.* **2009**, *13*, 36−45.

(93) Mukherjee, A.; Tothadi, S.; Desiraju, G. R. Halogen Bonds in Crystal Engineering: Like Hydrogen Bonds yet Different. *Acc. Chem. Res.* **2014**, *47*, 2514−2524.

(94) Nyburg, S. C.; Faerman, C. H. A revision of van der Waals atomic radii for molecular crystals: N, O, F, S, Cl, Se, Br and I bonded to carbon. *Acta Crystallogr. B* **1985**, *41*, 274−279.

(95) Stone, A. J.; Price, S. L. Some new ideas in the theory of intermolecular forces: anisotropic atom-atom potentials. *J. Phys. Chem.* **1988**, *92*, 3325−3335.

(96) Bui, T. T. T.; Dahaoui, S.; Lecomte, C.; Desiraju, G. R.; Espinosa, E. The Nature of Halogen···Halogen Interactions: A Model Derived from Experimental Charge-Density Analysis. *Angew. Chem., Int. Ed.* **2009**, *48*, 3838−3841.

(97) Spilfogel, T. S.; Titi, H. M.; Friščić, T. Database Investigation of Halogen Bonding and Halogen···Halogen Interactions between Porphyrins: Emergence of Robust Supramolecular Motifs and Frameworks. *Cryst. Growth Des.* **2021**, *21*, 1810−1832.

(98) Scheiner, S. Characterization of Type I and II Interactions between Halogen Atoms. *Cryst. Growth Des.* **2022**, *22*, 2692−2702.

https://doi.org/10.1021/acs.jpca.2c02451
J. Phys. Chem. A 2022, 126, 4025−4035